# The characteristics of sea fog with different airflow over the Huanghai Sea in boreal spring

HUANG Jian[1][*], WANG Xin[2], ZHOU Wen[2], HUANG Huijun[1], WANG Dongxiao[3], ZHOU Faxiu[4]

[1] Institute of Tropical and Marine Meteorology, China Meteorological Administration, Guangzhou 510080, China

[2] Guy Carpenter Asia-Pacific Climate Impact Centre, School of Energy and Environment, City University of Hong Kong, Hong Kong, China

[3] CAS key laboratory of tropical marine environmental dynamics, South China Sea Institute of Oceanology, Chinese Academy of Sciences, Guangzhou 510301, China

[4] Department of meteorology, Ocean University of China, Qingdao 262003, China

**Abstract**
Using the observations from ICOADS datasets and contemporaneous NCEP/NCAR reanalysis datasets during 1960-2002, the study classifies the airflows in favor of sea fog over the Huanghai (Yellow) Sea in boreal spring (April-May) with the method of trajectory analysis, and analyzes the changes of proportions of warm and cold sea fogs along different paths of airflow. According to the heat balance equation, we investigate the relationships between the marine meteorological conditions and the proportion of warm and cold sea fog along different airflow paths. The major results are summarized as follows. (1) Sea fogs over the Huanghai Sea in spring are not only warm fog but also cold fog. The proportion of warm fog only accounts for 44% in April, while increases as high as 57% in May. (2) Four primary airflow paths leading to spring sea fog are identified. They are originated from the northwest, east, southeast and southwest of the Huanghai Sea, respectively. The occurrence ratios of the warm sea fog along the east and southeast airflow paths are high of 55% and 70%, while these along the southwest and northwest airflow paths are merely 17.9% and 50%. (3) The key physical processes governing the warm/cold sea fog are heat advection transport, longwave radiation cooling at fog top, solar shortwave warming and latent heat flux between air-sea interfaces. (4) The characteristics of sea fog along the four airflow paths relate closely to the conditions of water vapor advection, and the vertical distribution of relative humidity.

**Key words:** spring sea fog over the Huanghai Sea, airflow paths, water vapor flux, heat advection, vertical distribution of water vapor

## 1 Introduction

Among Chinese offshore waters, sea fog occurs the most frequently over the Huanghai (Yellow) Sea. The Huanghai Sea fog is characterized by the vastness of area, large number of days of occurrence, extended duration of the fog season, and significant seasonal variations. Reducing both horizontal and vertical visibility over the sea and coasts, sea fog severely affects all means of transportation, which include marine fishing, rig drilling, commercial shipping, military operations, airplane flights and highway travel, and is one of the causes for serious accidents. Due to the limited observations at sea, which have hindered our understanding of the relevant physical properties and processes over the Huanghai Sea, operational forecast for sea fog remains insufficiently accurate to meet the needs of social and economic development (Wang, 1985).

Several air cooling progresses are responsible for the formation of fog. Warmer air could be cooling when meeting the cold sea surface (Taylor 1917; Byers 1930; Lamb 1943), or via turbulence exchanges (Petterssen, 1936; 1938), or via radiations (Emmons and Montgomery, 1947). However, once the fog formed, it might develop into two types of fog due to various synoptic patterns and marine meteorological conditions.

One is warm fog with the fog layer temperature higher than sea surface temperature (SST); and the other is cold fog with air temperature less than SST (Taylor, 1917). Warm fog and cold fog are both observed in different regions. Cold sea fog appears frequently along the coast of the British Isles and along the southern coast of California (Lamb, 1943; Pelie et al., 1979; Koracin et al., 2005), and sea fog shows the characteristics of warm fog over the Huanghai Sea, Japan Sea and the north of Pacific (Wang, 1985; Renard and Willms, 1975). Although both warm and cold fog result from the advection of warm air over cold sea surface, the associated physical mechanisms during their development and persistence phases are different from each other. The studies of cold fog have shown that longwave radiation at fog top is greatly associated with the cold fog formation, which plays important roles in fog development and persistence (Lamb, 1943; Findlater et al., 1989), and is referred to effect of sky conditions (Roach, 1995). In contrast, the importance of turbulent transport exchanges between air and sea is emphasized by Wang (1985) for the development and persistence of warm fog. Wang (1985) suggested that longwave radiation cooling at fog top in warm fog is not as important as in cold fog, which only thickens warm fog layer. The different physical progresses during warm and cold fog may influence the way of fog prediction.

Generally, the spring sea fog over the Huanghai Sea is known as the advection cooling fog resulting from warm and moist air to be transported advectively over cold sea surface (Wang, 1985; Zhou and Liu, 1986; Cho et al., 2000). Except for some front fog, advection cooling fog occurs frequently over the Huanghai Sea (Wang, 1985). Recently, it is suggested that sea fog over the Huanghai Sea shows the seasonal variations representing monsoon characteristics, especially in boreal spring of Asian monsoon transition period from winter monsoon to summer monsoon (Zhou and Wang, 2004; Wang et al., 2006; Zhang et al., 2009). However, it is still not clear that whether the sea fog over the Huanghai Sea in spring is warm fog or cold fog during sea fog development and persistence (Zhang and Ren, 2010), and what the marine meteorological conditions in favor of warm and cold fog formation, development, persistence and dissipation are.

The trajectory analysis of air mass is a usual and effective prediction method for sea fog (Taylor, 1917). Using the method of backward trajectory analysis, we can identify the originations of airflows, their thermal and dynamical characteristics, and their associated marine conditions (Wang, 1985; Lewis et al., 2003). Based on surface observations from ICOADS

datasets and contemporaneous NCEP/NCAR reanalysis datasets during 1960-2002, the prevailing paths of airflow resulting in fog over the Huanghai Sea in spring (April and May) are investigated by backward trajectory and cluster analysis, and the occurrence ratios of the warm and cold fog along each prevailing airflow path are examined. Besides, according to the heat balance equation, the key marine meteorological conditions associated with the warm and cold fog are discussed. The text is organized as the following. The data and methodology used in this study are introduced in Section 2. Section 3 analyzes the warm/cold fog ratios and associated heat and water vapor advection, and the vertical distribution of relative humidity along different path of airflow, and further investigates the physical mechanisms of fog maintenance. The conclusions are in Section 4.

## 2 Data and methodology

### 2.1 *Data*

The data used in this study include a 43-year (1960-2002) set of observations from the International Comprehensive Ocean-Atmosphere Data Set (ICOADS) compiled by the National Climate Data Center (NCDC) (Slutz et al., 1985; Woodruff et al., 1987; Bottomley et al., 1990). Being the most complete and comprehensive dataset of observations in the world, ICOADS is mainly comprised of measurements taken on commercial, military or research vessels, mooring buoys and other types of maritime platforms. The observations are made up of a series of independent texts that report on SST, wind direction, wind speed, air temperature, dew point temperature and weather phenomena in every three hours. Additionally, the contemporaneous NCEP/NCAR reanalysis datasets (Kalnay et al., 1996), which are available four times daily at $2.5° \times 2.5°$ grid points at 1000–200 hPa are used in this study.

Due to the marine environment and communication condition, surface reports from ICOADS are not always believable. In this study the rigid quality control processes are applied as follows. (1) Only highly reliable records, based on quality control mark of ICOADS, are available. (2) According to ship call letters, observed time, locations and content, the observed datasets are tested one by one. The duplicate reports and wrong reports on land were deleted. (3) The observation reports of the Huanghai Sea are tested by climatological means, referring that the variations of oceanic and atmospheric variables are limited in climatic ranges. For example, in this paper limits for SST, air temperature and sea level pressure are in

–2 °C to 40 °C, –50 °C to 50 °C, and 950 to 1050 hPa respectively. (4) Finally, the anomalies of variables are tested to ensure the reliability of the reports. For instance, air temperature reports are available only if the absolute values of the anomaly are less 10 °C. Detailed techniques for quality control and data verification are documented by Huang and Zhou (2006).

In this study, fog occurring in the central area of Huanghai Sea (32°–39°N, 121°–126°E) is chosen from ICOADS datasets because this area has the highest observation frequency (Wang et al., 2004). This choice also avoids the effect of coastal fog such as radiation fog (Huang and Zhou, 2006). In accordance with the specifications of the National Weather Service of U.S.A. for the use of ICOADS, fog is represented with the codes of 28, 41-47 if visibility is less than 1 km or with the codes of 10 and 12 if visibility is less than 1 km but the height of fog layer is less than 10m (NWS, 1991).The fully developed fog (codes 28, 41-47) have been picked out, and the light fog and shallow fog that is less than 10m in height (codes 10-12) were given up. In the central Huanghai Sea there are a total of 1137 records of sea fog for April and 2128 for May. In addition, if three or more fog records at different sites are reported at same time, then one sample of fog is identified. According to this threshold, there are 279 and 387 fog samples are determined in April and May, respectively.

## 2.2 *Methodology*

To investigate the characteristics of sea fog and associated marine meteorological conditions over the Huanghai Sea, the trajectories of air mass displacement for 279 and 387 fog samples in April and May are examined in this study. Based on the trajectory analysis, the cluster analysis is utilized to categorize the trajectories into typical airflow paths in accordance to the similarity principle. For the convenience of categorizing air mass trajectories, the point (124°E, 35°N) in the center of the Huanghai Sea, is assumed to be the starting point of airflow tracing because of the wide coverage of sea fog and relatively coarse resolution of the NCAR/NCEP reanalysis datasets.

Firstly, using the observations of ICOADS and NCEP/NCAR reanalysis wind field, the 36-h backward trajectory for each sea fog sample is computed by the backward trajectory analysis, which is described mathematically by Draxler (1996) as follows:

$$P(t + \Delta t) = P(t) + 0.5[V(p,t) + V'(p',t + \Delta t)]\Delta t$$
$$P'(t + \Delta t) = P(t) + V(p,t)\Delta t$$

Where $P(t)$ is the location of the trajectory at time $t$, $V(P,t)$ is the wind speed at time $t$ and point $P(t)$, $P'(t + \Delta t)$ is the location of the trajectory with the elapse of a time step of $\Delta t$, and $V'(P',t + \Delta t)$ is the wind speed at point $P'(t + \Delta t)$ with the elapse of a time step of $\Delta t$, which is derived by interpolation.

Secondly, the method of cluster analysis is used to categorize the air mass backward trajectories into limited number of airflow paths, which follows the principle of spatial and temporal similarity for multiple trajectories classification (Stunder, 1996).

Lastly, according to the airflow paths, the air-sea temperature difference associated sea fog in every airflow path is counted from ICOADS reports. And the transport of heat and water vapor at sea surface and the vertical distribution of relative humidity in every airflow path are also analyzed by composite method. As the composite is derived from real fog observations, it represents a schematic model with common characteristics of the path of airflow.

## 3 Main results

### 3.1 *The proportions of cold and warm fogs*

The air-sea temperature difference is one of the most important predictor of sea fog, which represents the thermal relationship between air and sea surface. Before sea fog formation, it is one of the important preconditions for air cooling and saturating. During development and persistence of sea fog, however, the air-sea temperature difference is the integrated result of heat balance among cooling and warming progresses (Findlater et al., 1989).

According to the definition of Wang (1985), in this paper sea fog is defined as warm fog in which air-sea temperature difference is between –0.1 and 5 °C and is defined as cold fog in which air-sea temperature difference ranges between –3 and –0.1 °C. The proportions of warm and cold fogs to all observation records are shown in Table 1.

**Table 1.** the proportions of warm and cold fog over the Huanghai Sea in spring (%)

| Month | Fog samples | Warm fog | Cold fog |
|-------|-------------|----------|----------|
| April | 279 | 44.1 | 55.9 |
| May | 387 | 57.6 | 42.4 |

It could be seen that not only warm fog but also cold fog occur over the Huanghai Sea in April and May. The proportion of warm fog in April is 44.1%, and that of cold fog is 55.9%. In May it is much different from those in April that the proportion of warm fog increases to 57.6%, and that of cold fog drops to 42.4%.

Besides, the proportions between warm and cold fog also show variation month by month. Warm fog increases with weakening winter monsoon during mid and late spring Wang (1985) suggested that fog over the Huanghai Sea is advection cooling fog or frontal fog, and 30% of fog is frontal fog. It is noted that the cold fog occurrence ratio in our statistical results is higher than that of Wang (1985). Due to the complexity of synoptic systems and associated marine meteorological conditions, the real physical mechanisms of sea fog over the Huanghai Sea in spring may be more complicated than our previous experiences. Except for evaporation fog or frontal fog, fog over the Yellow Sea could appear as cold fog while the advection cooling fog in its development and persistence stage (Taylor, 1917). To identify the above supposition, in the following sections the characteristics of airflows associated with fog and the ratios of warm and cold fog with these airflows are investigated.

### 3.2 The proportions of warm and cold fogs along different airflow paths

In this study, the airflow backward trajectories are computed for the 279 and 387 fog samples in April and May respectively, and the airflow backward trajectories are clustered into the airflow paths by cluster analysis.

Figure 1 shows the airflows associated with sea fog in April and May, respectively. For all of fog samples, the air mass trajectories in spring are eventually classified into four groups of airflow paths. That is to say, the four groups of airflows originating from different regions could lead to sea fog in spring. T-NW is a northwest airflow coming from the continental area; T-E is east airflow from the southern Korean peninsula or the Sea of Japan; T-SE is a southeast one from the northeast East China Sea or west Pacific; and T-SW is a southwest airflow from the western Huanghai Sea waters around 35°N or the east continent of China.
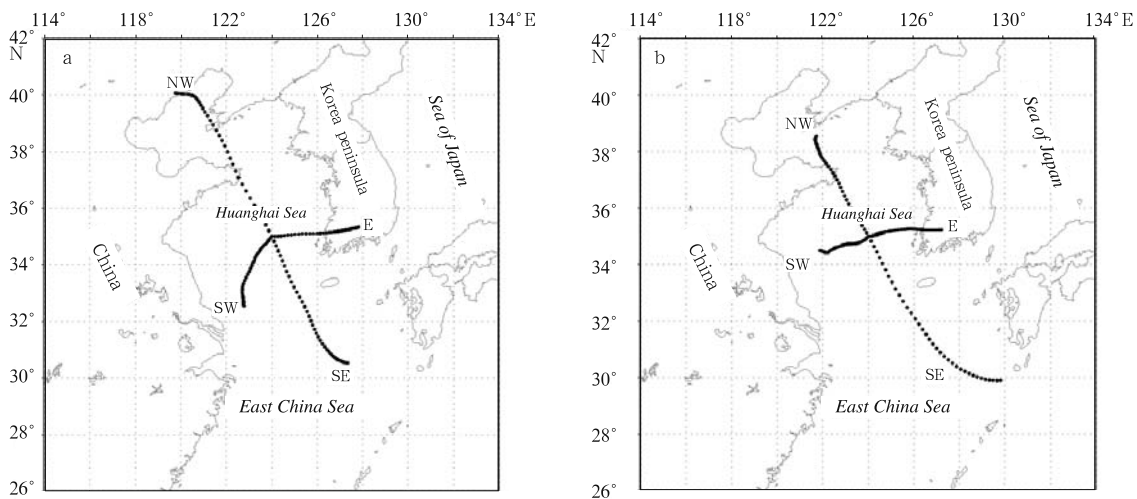


**Fig.1.** the airflows resulting in fog over the Huanghai Sea in a. April and b. May (The dot denotes the location of air mass in every hour).

In addition to significant differences in direction among the four airflow paths, Fig.1 also shows the difference of air mass moving speed. From the length of the four paths presented in Fig.1, it could be seen that the T-NW has the fastest moving speed among four airflow paths in April, while the T-SE becomes the fastest one in May. The percentages of four airflow paths show variations of month to month (Table 2). In April, the T-NW has the highest percentage (30.1%), followed by T-SE (27.3%). In May the percentage of the T-NW airflow substantially drops to 13.7% while that of the T-SE increases to 41.1% and the T-SE becomes the most frequent airflow. As the airflows are closely related to the circulation of synoptic regimes, the different ratios of the airflows reflect the atmospheric synoptic state changes during the East Asian monsoon transition period from winter monsoon to summer monsoon (Zhou and Wang, 2004; Wang et al., 2006).

**Table 2.** the percentages of airflow resulting in fog over the Huanghai Sea in April and May (%)

| Month | Path | | | |
|---|---|---|---|---|
| | T-NW | T-SW | T-E | T-SE |
| April | 30.1 | 21.1 | 21.5 | 27.3 |
| May | 13.7 | 18.6 | 26.6 | 41.1 |

**Table 3.** the proportions of warm and cold fog along different path of airflow (%)

| | T-NW | T-E | T-SE | T-SW |
|---|---|---|---|---|
| April | 17.9/82.1 | 55.9/44.1 | 68.3/31.7 | 44.7/55.3 |
| May | 47.2/52.8 | 66.7/33.3 | 69.9/30.1 | 49.1/50.9 |

The T-NW shows that air mass moves southwardly from the continent to the Huanghai Sea (Fig.1), which thus closely relates to the cold and dry air and frontal systems in spring. The fog mechanism for this path is more complicated than that of other paths, which is likely to be the evaporation fog resulting from cold and dry air mass, or frontal fog forming in the warm sector of frontal cyclone (Wang, 1985), even the advection cooling fog resulting from the warm and moist air mass which is modified by the underlying surface (Zhang and Ren, 2010). From Table 3, given air mass moving from the northern continental area, warm fog takes up 17.9% along the T-NW in April, and increase to 47.2% in May. It is speculated that in May the weakening of northerly cold and dry air mass (Zhou et al., 2004) is the possible reason for higher ratio of warm fog along T-NW.

The T-SW is a southwest or west airflow origin in the Huanghai Sea or adjacent waters, which was less mentioned in previous literatures. The ratios of warm fog along T-SW in April and May are 44.7% and 49.1%, respectively. This airflow is characterized by the slowest moving speed among four airflow paths of, and results in almost the same ratios of warm and cold fog in April and May.

The T-E and T-SE are the most popular airflows associated with sea fog over the Huanghai Sea (Wang, 1985; Wang et al., 2004). These two paths of airflow are characterized by the high ratios of warm fog and the significant month-to-month changes. For the T-E warm fog takes up 55.9% in April, and increases to 66.7% in May. For the T-SE the ratios of warm fog in April and May are as high as 68.3% and 69.9%. With the weakening East Asian winter monsoon from April to May, the ratios of warm fog in four paths are higher in May than those in April, indicating the seasonal change during the period of Asian monsoon transition from winter to summer monsoon.

The above results indicate that the characteristics of sea fog over the Huanghai Sea in spring are associated closely with the airflows originating different regions. Since the T-NW usually relates to frontal systems or cold and dry air over the continent the characteristics of fog along this airflow path is complicated. The occurrence ratio of cold fog along T-SW airflow path is relatively high. In contrast, the T-E and T-SE airflow paths are in favor of occurrence of warm fog. It is clear that the characteristics of fog depend on the marine meteorological conditions along these airflows.

### 3.3 The key physical progresses influencing characteristics of sea fog

Sea fog is the phenomenon that the water vapor condenses into tiny liquid water droplets in the marine atmospheric boundary layer, which is governed by complicated micro physical processes in its formation, development and persistence. Sea fog is involved with these physical processes of turbulent transportation, radiation effect, settlement of fog droplets, entrainment at fog top and so on (Lewis et al., 2004). Little has been known of the effects of these physical processes on heat and water vapor balance in different sea fog. Especially, there is little knowledge about how these physical processes influence the air-sea temperature difference in the lowest layer of fog.

Using the heat balance equation given by Nicholls (1984) and Findlater et al. (1989), the following discusses the main physical processes associated with warm and cold fog. The heat balance equation for sea fog layer given by Nicholls (1984) is:

$$h(d\theta_e/dt) = \theta_0 + \theta_h + S + u\nabla T_a + R_o - R_h \qquad (1)$$

where $h$ is thickness of sea fog layer; $\theta_e$ is equivalent potential temperature; $\theta_o$ and $\theta_h$ are turbulent fluxes of $\theta_e$ at surface and fog top, respectively; $S$ is total absorption of solar radiation within fog layer; $u\nabla T_a$ is advection of heat; $R_o$ and $R_h$ are net longwave radiation at sea surface and fog top. $\theta_e = \theta + L/c_P q, \theta$ is potential temperature, $L$ is latent heat flux and $c_p$ is specific heat at constant volume of air mass.

Air-sea temperature difference and air-sea specific humidity difference are defined as:

$$\Delta T = T_s - T_o, \Delta q = q_{sat}(T_s) - q_o$$

where $T_s$ and $T_o$ indicate SST and surface air temperature; $q_o$ and $q_{sat}(T_s)$ are vapor mixing ratio of air and saturated vapor mixing ration at $T_s$.

Besides, we define

$$(\theta_e)_s = \theta_e + (\Delta\theta_e)_o = \theta_s + Lq_{sat}(T_s)/C_p \qquad (2)$$

$$(\Delta\theta_e)_o = (\Delta\theta_e)_o + (L/c_p)(\Delta q)_o \approx$$
$$(\Delta T)_o + (L/c_p)(\Delta q)_o \qquad (3)$$

According to Eq. (2), the term on the left hand in Eq. (1) is changed into: $d\theta_e/dt = d(\theta_e)_s/dt - d(\Delta\theta_e)_o$

Moreover, due to Eq. (3), $d\theta_e/dt = d(\theta_e)_s/dt - Xd(\Delta T)_o/dt$

Where $X = 1 + (L/c_p)(dq_{sat}/dt); d(\theta_e)_s/dt \approx dT_s/dt$ is the variation of SST with time.

The terms on the right hand in Eq. (1) are explained detail by detail in the following.

$\theta_o$, the first term on the right hand side of Eq. (1), is sensible and latent heat flux between air and sea.

$$\theta_o = H_o + (L/c_p)E_o = c_h u(\Delta T)_o + (L/c_p)c_q u(\Delta q)_o$$

where $H_o$ and $E_o$ are sensible and latent heat flux from sea surface, respectively; $c_h$ and $c_q$ are aerodynamic bulk exchange coefficient for heat and water vapor, respectively; and $u$ represents sea surface wind speed.

$\theta_h$, the second term on the right hand of Eq. (1), is entrainment sensible and latent heat fluxes at fog top

$$\theta_h = H_h + (L/c_p)E_h = w_e[H_h + (L/c_p)(\Delta q)_h]$$

Since vapor content at fog top is near zero and $(\Delta q)_h$ is small, the term of latent heat can be omitted. In view of $H_h/H_o$ the value of being about 1.4-2.0, the term of sensible heat can be expressed by $H_h = a_o H_o$, where the coefficient $a_o$ is about 1.4 to 2.0 (Findlater et al., 1989). Thus, $\theta_h$ can be written as:

$$\theta_h = a_o H_o$$

$S$, the third term on the right hand side of Eq. (1), is total solar shortwave radiation absorbed by fog layer, which is only valid during daytime.

Given the sea surface and fog layer as blackbodies $R_o$, the fourth term on the right hand side of Eq. (1), can be approximated as

$$R_o = 4\sigma T^3 (\Delta T)_o$$

Finally, without local SST gradient, Eq. (1) can be rewritten as

$$hXd(\Delta T)_o/dt = -c_h u(1 + a_o)(\Theta T)_o - (L/c_p)c_q$$
$$u(\Delta q)_o - S - u(\nabla T) - 4\sigma T^3(\Delta T)_o + R_h \quad (4)$$

As the heat in fog layer tends to be in a state of balance or quasi-equilibrium(Findlater et al., 1989), meaning $d(\Delta T)_o/dt = 0$, Eq.(4) can be written as

$$(\Delta T)_o = \frac{R_h - S - (L/c_p)c_q u(\Delta q)_o - u(\nabla T)_a}{c_h u(1 + a_0) + 4\sigma T^3} \quad (5)$$

According to Eq.(5), the sign of temperature difference between air and sea $(\Delta T)_o$ is dependent on longwave radiation at fog top $R_h$, total solar radiation absorbed by fog layer $S$, latent heat flux $-(L/c_p)c_q u(\Delta q)_o$ and the advection of heat $-u(\nabla T)_a$. The terms of sensible heat $c_h u(1 + a_0)$ and longwave radiation between air and sea surface $4\sigma T^3$ can only influence on magnitude of air-sea temperature difference.

Different from longwave radiation at fog top, the total shortwave radiation absorbed by fog layer depending on the solar altitude angle and can't always warm the fog layer. It works only during daytime and reaches its maximum at noon. However, the magnitudes of $S$ and $R_h$ are relative constant,

and the daily average of $S$ only accounts for 20% of $R_h$ (Findlater et al. 1989). Therefore, the sign of $(\Delta T)_o$ depends largely on the relative magnitudes of $R_h, -(L/c_p)c_q u(\Delta q)_o$, and $-u(\nabla T)_a$.

$$(\Delta T)_o = \frac{R_h - (L/c_p)c_q u(\Delta q)_o - u(\nabla T)_a}{c_h u(1 + a_0) + 4\sigma T^3} \quad (6)$$

## 3.4 The marine meteorological conditions of four airflow paths

### 3.4.1 The characteristics of heat advection flux

According to Eq. (6), it is known that heat advection, $-u(\nabla T)_a$, is an important factor governing warm or cold fog occurrence. Obviously, it is conducive to warm fog when the there is strong heat transport; and it tends to be cold fog when the heat transport is weak or negative. To identify the relationship between fog and marine meteorological condition, here we use the surface air temperature and wind speed from ICOADS data to calculate the heat advections of each sea fog sample and composite fields of each airflow path. As the heat advections in April are similar to that in May, only the heat advections in May are presented.

For T-NW airflow, the heat advection is positive over the Bohai Sea, and is almost negative over the Huanghai Sea (Fig.2a). The heat can be transported advectively into the Huanghai Sea along T-SW airflow, especially over the west of the Huanghai Sea, but its magnitude is small (Fig.2d). Fig. 2b shows that the magnitude of heat advection for T-E airflow is much larger than that for T-SW airflow, and its maximal centre locates over the central of the Huanghai Sea. The heat advection for T-SE airflow is the largest in the four paths of airflow (Fig.2c). According to Table 3, the ratios of warm fog along T-SE is the largest as high as 69.9%, followed by T-E (66.7%) and T-SW(49.1%), and is the smallest with T-NW (47.2%), which is consistent with the magnitudes of heat advection.

Many observed evidences have shown that warm fog tends to occur in strong warm air advection (Wang, 1985; Zhou and Liu, 1986), whereas cold fog appears when warm advection weakens or ceases (Taylor 1917; Lamb 1943), which is consistent with the above results of heat advection for four airflow paths.

### 3.4.2 The characteristics of water vapor flux

In warm fog air temperature is warmer than sea surface temperature by several degrees, and in cold fog it is 1–2 degrees colder than sea surface temperature (Taylor 1917). Previous studies suggested that air in warm fog is dried and cooled via turbulent exchanges between air and sea (Roll, 1965), and air in cold fog is warmed and moistened because of the heat and water
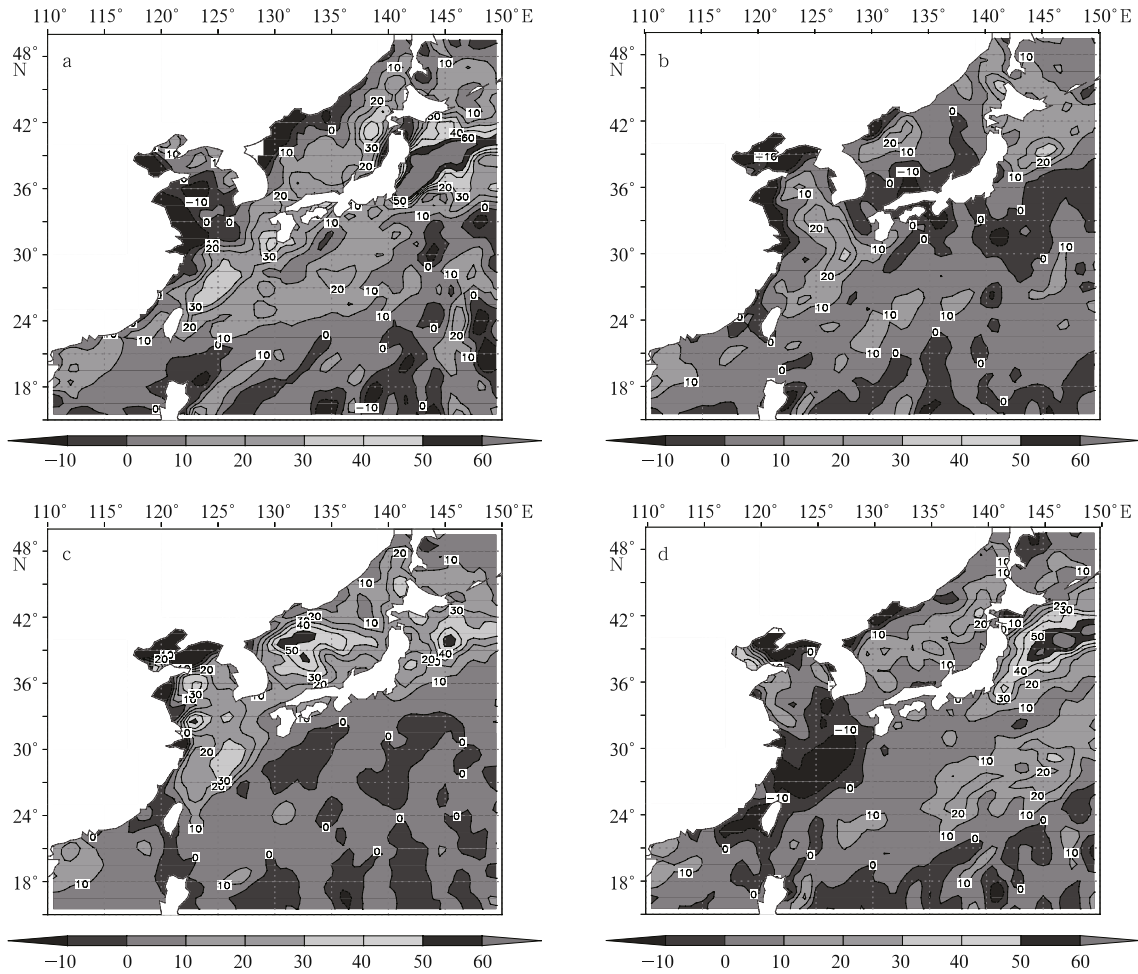
**Fig.2.** the heat advection of (a)T-NW,(b) T-E, (c) T-SE and (d) T-SW path of airflow in May (Units: $Kms^{-2} \times 10^{-6}$) (The contours denote the magnitude of flux).

vapor transportation near sea surface (Findlater et al., 1989). The temperature and water vapor of air is regulated by the sea through the turbulent exchanges and tends to be the same at air-sea interface the (Leipper, 1994). The gradient of water vapor in latent heat flux term, $-(L/c_p)c_q u(\Delta q)_o$, therefore, primarily a result of water vapor transportation by synoptic circulations.

The horizontal water vapor flux could represent the transportation and source of water vapor in large scale. With sea surface wind fields and specific humidity data from ICOADS, the water vapor fluxes near sea surface during fog along four airflow paths are calculated respectively. The equation used for this calculation is $-\overrightarrow{V} \cdot q \cdot \Delta p$, where $\overrightarrow{V}$ is the vector of the horizontal wind, $q$ is specific humidity, and $\Delta p$ is the difference in vertical air pressure, which is taken to be 1 hPa in this work. As the water vapor flux is similar between April and May, only the figures in May are given here (Fig. 3).

With different sources of airflow, the water vapor flux differs dramatically (Fig.3). There is little water

vapor to be transported to the Huanghai Sea because air mass along the T-NW airflow originates from winter monsoon synoptic system and northern continent (Fig. 3a). Less water vapor is transported along the T-SW airflow, although it originates from southwest or west of the Huanghai Sea (Fig. 3d). Coming from Korean peninsula or the Sea of Japan to the Huanghai Sea, T-E is an airflow that conveys water vapor just less than that of T-SE but more than that of T-NW or T-SW (Fig. 3b).Originating from the southeast, T-SE airflow carries water vapor into the Huanghai Sea from the East China Sea or the northwest of Pacific (Fig. 3c). It is noted that the water vapor flux along T-SE is much more than that along the other three airflows.

It is known that the signs of the temperature and water vapor gradient at near surface level are the same when air is in saturated state. The strong water vapor transportations along T-SE and T-E are helpful for maintaining the gradient of water vapor, and thus in favor of occurrence of warm fog. Due to the condensa-
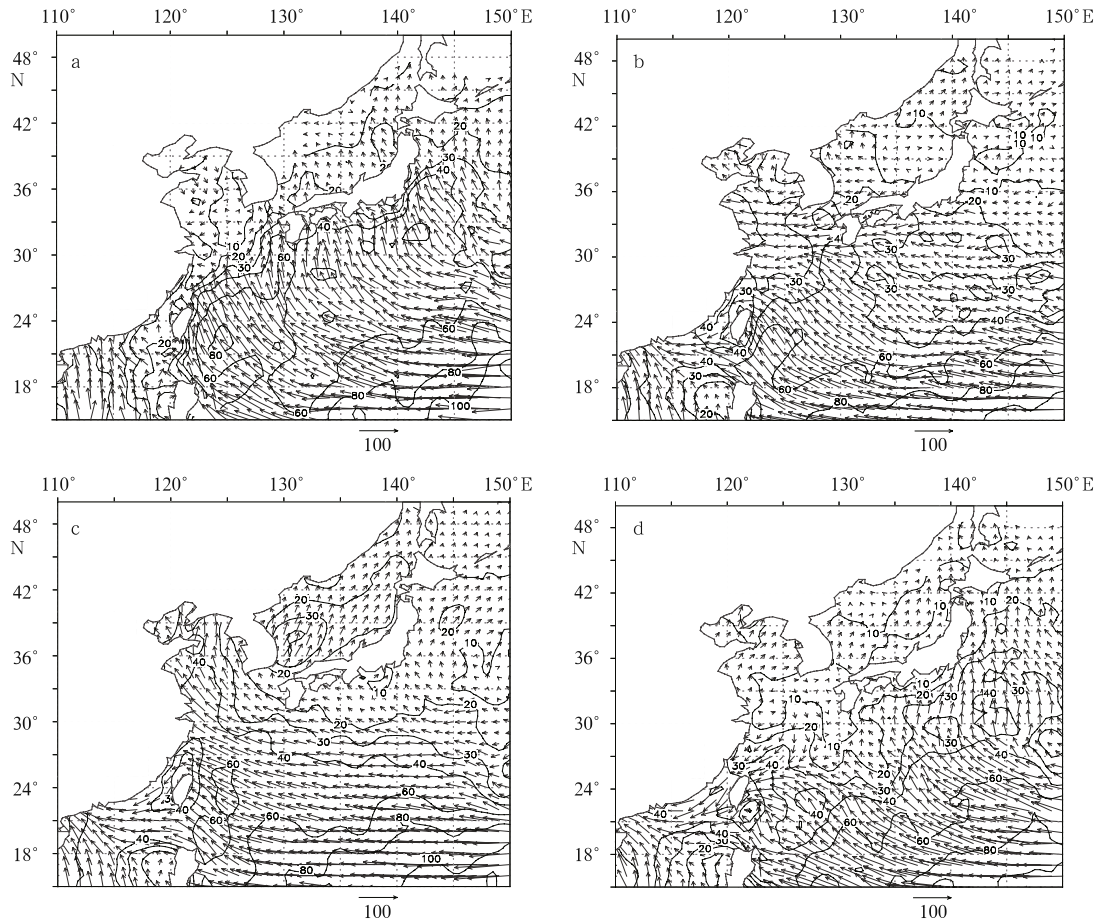
**Fig.3.** the water vapor advection flux of (a) T-NW, (b) T-E, (c) T-SE and (d) T-SW paths of airflow in May (Units: g·m$^{-1}$·hPa$^{-1}$·s$^{-1}$·10$^{-4}$) (The vectors stand for the magnitude and direction of flux, and the contours denote the magnitude of flux).

tion of water vapor and settlement of fog droplets, water vapor content in fog layer will decrease when there is weak transportation of water vapor. Fog will dissipate, or persist through the continuous cooling of longwave radiation until air temperature less than sea surface temperature, and the evaporation from sea surface to offset the loss of water vapor.

### 3.4.3 Characteristics of vertical distribution of relative humidity

Longwave radiation at fog top, $R_h$, depends on the difference between the upward longwave radiation emitted at fog top and the downward longwave radiation of atmosphere. According to Angstrom empirical formula (Angstrom, 1912), $R_h = \sigma T_h^4(A - B \cdot 10^{-re})$, where $T_h$ is the temperature of fog top; $\sigma$ is Stefan-Boltzmann constant; $e$ is water vapor pressure; $A, B$, and $r$ are correction coefficient relating greatly with cloud form and cover. Evidently, $R_h$ is dependent on the sky condition and has close relationship with the vertical distribution of relative humidity.

It is noted that the humidity in NCEP/NCAR reanalysis is less reliable than winds, pressure and temperature. However this reanalysis dataset is the only long-term dataset available in recent years, and it does reflect the characteristics of large-scale synoptic regimes to some extent. Figure 4 is the composite vertical distributions of relative humidity along 125°E for the four airflow paths in May. The Huanghai Sea is located between 33 and 39°N. Since the vertical distribution of relative humidity in April is very similar to that in May, only patterns in May are shown.

Figure 4 shows the vertical distributions of relative humidity for four airflow paths. It is clear that the vertical distributions of relative humidity connect closely with the water vapor transportations. For T-NW and T-SW airflow paths there are weak water vapor transportations and extremely dry layer are observed (Figs 4a and d), and for T-E and T-SE there are strong water vapor transportation and deeper layer of the high relative humidity(Figs 4b and c). This connection could be explained as follows. For T-NW and T-SW airflow paths, once fog occurs, the water vapor of fog largely depends on evaporation at sea surface because of weak water vapor transportation. Simultan-
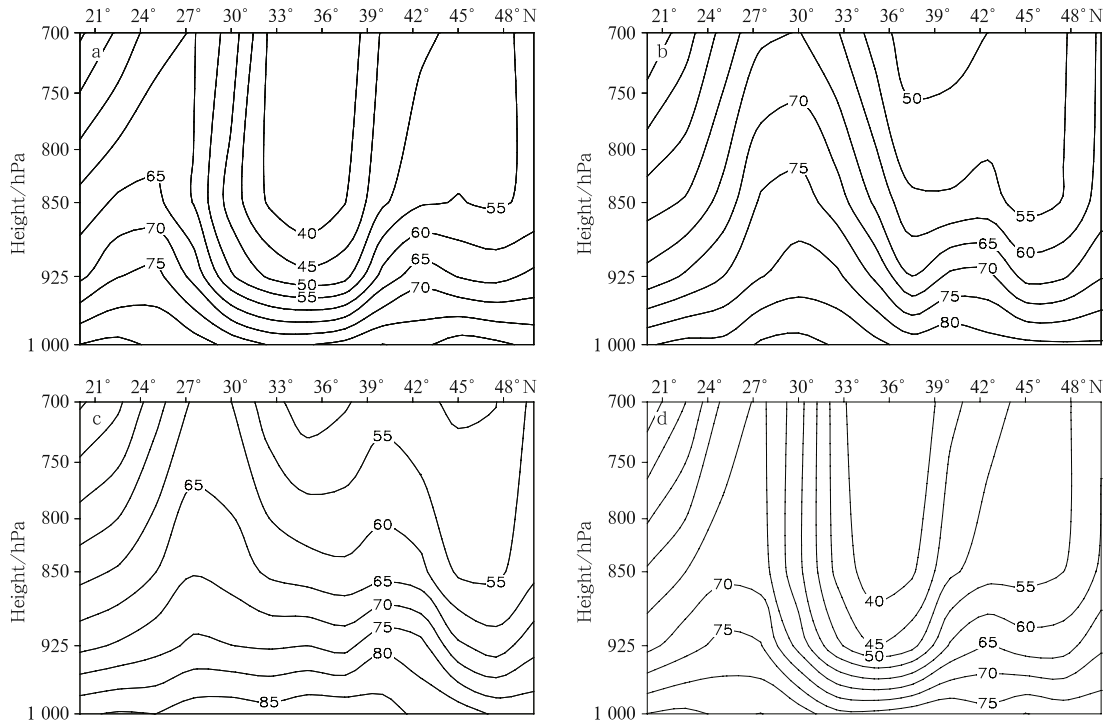
**Fig.4.** the vertical distributions of relative humidity of (a)T-NW,(b) T-E, (c) T-SE and (d) T-SW paths of airflow in May (%) (The Huanghai Sea is located between 33°N and 39°N).

eously, clear sky and more dry air at high level increase the longwave radiation cooling at fog top and evaporation at sea surface, which is evidently in favor of fog maintenance. However, for T-E and T-SE airflow paths, the strong water vapor transportations cause the high relative humidity at high level. The resulting larger vapor pressure decreases the efficiency of the longwave radiation cooling. On the other hand, it is very likely to form cloud layers over fog layer and cut off the heat transport to outer space by fog-top longwave radiation. Therefore, the patterns of water vapor advection and vertical distribution of relative humidity at lower level troposphere may be the key factors determining whether sea fog is cold fog or warm fog.

## 4 Conclusions

Based on the data from ICOADS and NCEP/NCAR reanalysis datasets, the characteristics of sea fog along different airflow paths over the Huanghai Sea in spring are investigated. The marine atmospheric conditions associated with four airflow paths are also discussed according to the heat balance equation. The main results are the following:

(1) The airflows resulting in sea fog over the Huanghai Sea in spring have four distinctive paths: the northwest airflow from the continental area to the north Huanghai Sea, the east airflow from the southern Korean peninsula, the southeast airflow from the northeast East China Sea, and the southwest airflow from the western Huanghai Sea waters around 35°N.

(2) The fog over the Huanghai Sea in spring can evolve as warm fog or cold fog. The ratios of warm and cold fogs vary with the airflow paths, and show variation in April and May. The ratio of warm fog in May is higher than that in April, and varies with the seasonal transition from winter monsoon to summer monsoon.

(3) The ratios of warm fog with the T-E and T-SE paths of airflow are about 55% to 70%, whereas that with the T-SW and T-NW airflow path is less than 50%, especially with T-NW in April, which is only 17.9%.

(4) The characteristics of sea fog are related to the heat and water vapor advection, longwave radiation at top fog layer, total solar shortwave radiation absorbed by fog layer, latent heat exchanges between air and sea, and so on. Our results suggest that the most important physical processes of spring sea fog over the Huanghai Sea are the magnitudes of water vapor advection and vertical distribution of relative humidity.

(5) The water vapor transportations with T-E and T-SE paths of airflow are much more, which is favorable for warm fog. However, with the condition of weak water vapor advective transportation for T-SW and T-NW airflow paths, the strong outgoing longwave radiation at fog top leads to more probability of cold fog.

## References

Angstrom A. 1912. Note on the relation between time of sunshine and cloudness in Stokholm, 1908-20 Archiv Matemat Astronom and Physik. B17, No 15

Bottomley M, Folland C, Hsiung J, et al. 1990. Global Ocean Surface Temperatures Atlas (GOSTA). Joint Meteorological Office and Massachusetts Institute of Technology Project, 20 +iv pages, and 313 plates

Byers H. 1930. Summer sea fogs of the central California coast. Publ Geogr, 3: 291–338

Cho Y, Kim M, Kim B. 2000. Sea fog around the Korean Peninsula. J Appl Meteo, 39: 2473–2479

Draxler R R. 1996. Trajectory optimization for balloon flight planning. Weather and Forecasting, 11: 111–114

Emmons G, Montgomery R. 1947. Note on the physics of fog formation. J Meteor, 4: 206 Findlater J, Roach W, McHugh B. 1989. The haar of north-east Scotland. Quart J Roy Meteor Soc, 115: 581–608

Huang Jian, Zhou Faxiu. 2006. The cooling and moistening effect on the formation of sea fog in the Huanghai Sea. Acta Oceanologica Sinia, 25(2): 49–62

Kalnay E, Kanamitsu M, Kistler R, et al. 1996. The NCEP/NCAR 40-year reanalysis project. Bull Amer Meteor. Soc., 77:437–470.

Koracin D, Leipper D F, Lewis J M. 2005. Modeling sea fog on the U.S. California coast during a hot spell event. Geofizika, 22: 59–82

Lamb H. 1943. Haars or North Sea fogs on the coasts of Great Britain. Meteorology Office Publication M O. 504: 24

Leipper D. F. 1994. Fog on the United States West Coast: a review. Bull. Amer Meteor Soc, 75: 229–240

Lewis J, Koracin D, Rabin R, et al. 2003. Sea fog along the California coast: Viewed in the context of transient weather systems. J Geophys Res, 108, 4457, doi:10.1029/2002JD002833

Lewis J, Koracin D, Redmond K. 2004. Sea Fog Research in the United Kingdom and United States. Bull Amer Meteor Soc, 82: 395–408

National Weather Service. 1991. National Weather Service Observing Handbook No.1, Marine Surface Weather Observations, Untied States Dept. of Commerce, NOAA, National Weather Service, Sliver Spring, Maryland

Nicholls S. 1984. The dynamics of stratocumulus: Aircraft observations and comparison with a mixed layer model. Quart J Roy Meteor Soc, 110: 783–820

Petterssen S. 1936. On the causes and the forecasting of the California fog. J Aerosp Sci, 3: 305–309

Petterssen S. 1938. On the causes and the forecasting of the California fog. Bull Amer Meteor Soc, 19: 49-55

Pilie R J, Mack E J, Rogers C W, et al. 1979. The formation of marine fog and the development of fogstratus systems along the California coast. J Appl Meteor, 18: 1275–1286

Renard R J, Willms G R. 1975. A climatology of marine fog frequencies for the North Pacific Ocean summer fog season. M.S. thesis, Department of Meteorology, NPS, 55

Roach W T. 1995. Back to basics: Fog: part 3-The formation and dissipation of sea fog. Weather, 50: 80–84

Roll H U. 1965. Physics of marine atmosphere. International Geophysics Series, 7: 352–367

Slutz R J, Lubker S J, Hiscox J D, et al. 1985. Comprehensive ocean atmosphere data set: Release 1. NOAA Environmental Research Laboratories, Climate Research Program, Boulder, CO, 268

Stunder B. 1996. An assessment of the quality of forecast trajectories. J Appl Meteor, 35: 1319–1331

Taylor G. 1917. The formation of fog and mist. Quart J Roy Meteor Soc, 43: 241–268

Wang Binhua. 1985. Sea Fog. Beijing: China Ocean Press, 352

Wang Peigao, Liu Zongyi, Zhang Kaitou. 2004. Applied Satellite Meteorology (in Chinese). Qingdao: Ocean University of China Press, 232

Wang Xin, Huang Fei, Zhou Faxiu. 2006. Climatic characters of sea fog formation of the Huanghai Sea in summer (in Chinese). Acta Oceanologica Sinica, 28: 26–34

Woodruff S, Slutz R, Jenne R. 1987. A comprehensive ocean-atmosphere dataset. Bull Amer Meteor Soc, 68: 1239–1250

Zhang Suping, Xie Shangping, Liu Qinyu, et al. 2009. Seasonal Variations of Huanghai Sea Fog: Observations and Mechanisms. Journal of Climate, 22: 6758–6772

Zhang Suping, Ren Zhaopeng. 2010. The influence of thermal effects of underlying surface on the spring sea fog over the Huanghai Sea: Observations and numerical simulation (in Chinese). Acta Meteorologica Sinica, 68(1): 115–125

Zhou Faxiu, Liu Longtai. 1986. Sea fog (The report of comprehensive investigation for the adjacent seas of the mouth of Changjiang River and Jeju Island). Acta Shandong Institute of Oceanography (in Chinese), 16(1): 115–131

Zhou Faxiu, Wang Xin. 2004. Climatic Characteristics of Sea Fog Formation of the Huanghai Sea in Spring (in Chinese). Acta Oceanography Sinica26(3): 28–37